International Journal of Lightweight Materials and Manufacture 6 (2023) 149–164

Contents lists available at ScienceDirect

International Journal of Lightweight Materials and Manufacture

journal homepage: www.keaipublishing.com/ijlmm

Original Article

Machinability and surface integrity investigation during helical hole milling in AZ31 magnesium alloy

Raviraja Adhikari [a], Gururaj Bolar [a,*], Ragavanantham Shanmugam [b], Ugur Koklu [c]

[a] Department of Mechanical & Industrial Engineering, Manipal Institute of Technology, Manipal Academy of Higher Education, Manipal, 576 104, India
[b] School of Engineering, Math & Technology, Navajo Technical University, NM 87313, USA
[c] Department of Mechanical Engineering, Faculty of Engineering, Karamanoglu Mehmetbey University, 70100, Turkey

ARTICLE INFO

Article history:
Received 3 July 2022
Received in revised form
7 September 2022
Accepted 18 September 2022
Available online 23 September 2022

Keywords:
Helical milling
Magnesium alloy
Cutting force
Surface roughness
Microhardness

ABSTRACT

Conventional drilling has been widely used for making holes in structural materials. However, drawbacks like high cutting forces, poor surface finish, high cutting temperatures, excessive tool wear, and undesirable burr formation while drilling magnesium alloys have necessitated the development of alternative hole-making methods. Lately, the helical milling process has attracted interest in facilitating hole-making for assembly applications. However, the machinability of magnesium alloys using the helical milling process needs more investigation. Therefore, the presented work analyzed the influence of axial pitch, tangential feed, and spindle speed on cutting forces and surface integrity while milling AZ31 magnesium alloy. Axial feed was the most crucial factor contributing to the thrust force (71.8%), followed by tangential feed (13.2%). All three process variables impacted the radial force. Spindle speed was the most influential variable affecting the surface roughness (48.7%), followed by axial pitch (31.4%) and tangential feed (12.5%). Microhardness closer to the free surface of the hole was higher than the subsurface hardness. Moreover, microhardness showed an upward trend with the rise in axial pitch and tangential feed; however, it reduced with increased spindle speed.

1. Introduction

The unending need by the automotive, aeronautical, and aerospace industries to minimize energy consumption has led to the development of several lighter materials. In this context, magnesium and its alloys have gained popularity considering the low density, high specific stiffness [1], specific strength [2], and excellent damping properties [3]. The displayed properties make magnesium alloys a competitive structural material. When used as a material for structural applications, machining operations become essential. Traditional drilling is popularly used for hole-making in structural applications where parts are assembled by riveting and screwing.

Several research groups have explored the process of dry drilling of magnesium alloys. Chong and Shih [4] gauged the effects of feed rate, spindle speed, and point angle on surface roughness and cutting forces while drilling AZ61A magnesium alloy. Surface roughness and cutting forces increased as the point angle increased. Moreover, a smaller point angle increased the resistance force and heat generation rate, producing built-up edges and raising the likelihood of chip ignition. A drill with a 55° point angle was recommended as it helped in improving the surface finish. Wang et al. [5] experimentally investigated the tool wear phenomenon while drilling magnesium alloy using High-Speed Steel (HSS) tools under dry cutting conditions. The wear map was developed considering the changes in wear rate and surface morphology. The wear map revealed the presence of five wear zones while dry drilling AZ91 magnesium alloy. The research determined diffusion, abrasion, and adhesive wear as the principal mechanisms. Bhowmick et al. [6] deliberated on the drilling of magnesium alloy (AM60) using HSS twist drills under dry and Minimum Quantity Lubrication (MQL) conditions. It was reported that the transfer of soft material onto the tool led to prominent built-up edges (BUEs) and consequently increased the torque and thrust force during dry drilling. Moreover, dry drilling decreased the tool life due to excessive material adhesion. However, using MQL helped reduce the cutting temperature and material adhesion

* Corresponding author.
E-mail address: gururaj.bolar@manipal.edu (G. Bolar).
Peer review under responsibility of Editorial Board of International Journal of Lightweight Materials and Manufacture.

https://doi.org/10.1016/j.ijlmm.2022.09.006

and improved the tool life. Berzosa et al. [7] analyzed the hole drilling process in UNSM11917 magnesium alloy, considering the surface roughness under dry machining conditions. Using drills with a 135° point angle and a lower cutting speed resulted in a poor surface finish. Additionally, microscopic inspection revealed the presence of adhered material at the margins of the drills when lower feed rates and higher cutting speeds were employed. Agustina et al. [8] evaluated the point angle, feed rate, and cutting speed when drilling magnesium alloy. Feed rate and cutting speed were reported to be influential, with the superior surface finish being achieved at higher speed and lower feeds. However, the presence of long chips deteriorated the hole surface quality. The selection of drills with a 135° point angle yielded poor surface quality. Research carried out by Koklu et al. [9] on the drilling of magnesium alloy reported that 2-flute drills helped lower the thrust force, whereas the 3-flute drills showed lower tool wear. Microstructural analysis revealed the refinement of grains due to higher cutting temperatures. Moreover, microhardness at the bore surface was higher than the bulk hardness, and the holes drilled with a 2-flute cutter showed higher hardness than a 3-flute cutter.

A few researchers have explored the influence of material composition and production techniques on the machinability of magnesium alloys during the drilling process. Sunil et al. [10] carried out drilling operations on AZ31 and AZ91 magnesium alloys and assessed the impact of the secondary phase (Mg17Al12) on their machinability. The secondary phase impacted the machinability by drastically increasing the cutting force magnitude. Yazman et al. [11] carried out high-speed drilling on cold chamber die-cast AZ91 magnesium alloy. The thrust force increased substantially with the feed rate. Also, high-speed conditions resulted in excessive tool wear. Additionally, the formation of folded chips was noted, which obstructed the drilling process and increased the temperature in the cutting zone by increasing friction.

The feasibility of using tool coatings to improve the machinability of magnesium alloys and overcome the limitations of the dry drilling process has been researched. Gariboldi [12] investigated the process of hole drilling in AM60B magnesium alloy with uncoated and coated drills. The HSS drills were coated with TiN, CrN, and ZrN materials. Uncoated tools allowed the built-up edge (BUE) to form, thus lowering the tool life. In contrast, the coated tools performed better within a range of optimal feed values. Bhowmick et al. [13] evaluated the effect of tool coating on magnesium drilling characteristics considering dry and MQL conditions. High cutting temperature promoted material softening and BUE formation leading to higher torque and flank wear. As expected, both coated and non-hydrogenated diamond-like carbon (NH-DLC) coated HSS drills failed prematurely under dry machining conditions due to excessive cutting temperatures. However, the utilization of MQL helped improve the tool life due to the reduced magnitude of the machining temperature. Karaca and Aksakal [14] evaluated the drilling performance of HSS and TiBN-coated drills while dry machining MA8M Mg alloy. Analysis showed that lower spindle speed and feed rates lead to higher surface-roughness values. Additionally, higher cutting speed led to higher cutting temperatures, reducing cutting performance and surface integrity. The evaluated TiBN coating was unsuitable for drilling MA8M magnesium alloy as it exhibited undesired surface qualities.

Recently, the cryogenic cooling technique has been utilized to overcome the limitations of the dry drilling process. Kheireddine et al. [15] developed a finite element method (FEM) model to analyze the cryogenic cooling process while drilling by considering the surface hardness. The cryogen-assisted drilling resulted in higher hardness as compared to dry drilled holes. Koklu and Coban [16] explored the process of dry and cryogenic drilling of magnesium alloy. Cryogenic drilling helped in lowering the material adhesion as compared to dry drilling. However, thrust force increased substantially due to the microstructural alteration during cryogenic drilling.

Magnesium alloys have excellent machinability; however, as reported, several drawbacks exist, especially while drilling under dry conditions. Dry drilling of magnesium alloys has shown an inclination towards the formation of BUE, thus lowering the tool life. Dry drilling generally produces a high thrust force value, which can damage the cutting tool and limit the productivity of the process. Besides, the dimensional accuracy and integrity of the surface processed holes are adversely affected by the regressive frictional characteristics at the work-tool-chip interface. To some extent, the utilization of MQL helped solve the issues, including chip adhesion and high temperature. Even though MQL has been successful in providing improved lubrication conditions, the cooling capacity of the process was found to be wanting when processing deep holes compared to the flood cooling system [17,18]. Also, the chip flushing capability of MQL was found to be inefficient [19]. The ineffective cooling rate is also the main reason for roll-back-type burrs [20]. If conventional cutting oils are used, the oil can adhere to the chip, thus reducing the recycling potential of the material. Similarly, cryogenic machining is considered a green manufacturing process. But it has been reported that using cryogens increases the work material strength and hardness, which can result in excessive abrasive wear of the drill bit [21]. Moreover, the production of cryogens like LN_2, being an energy-intensive process, contradicts the sustainability principles [22]. In addition, the use of CO_2 as a cryogen can be problematic since the accumulation of the gas on the shop floor can cause oxygen deficiency. Furthermore, improper handling of the coolant without proper safety gear can cause hazardous frostbite, thereby posing a health risk [23]. Besides, the high initial investment to set up the cooling system and the expendable nature of the cryogen increase the production cost [24]. Since drilling accounts for a significant share of all machining operations (40%) [25], an obligation exists to make the hole-making process sustainable.

In pursuit of sustainability, researchers evaluated the scope of helical milling to produce holes in various materials. Fig. 1 demonstrates the helical milling kinematics. The process has a rotating end mill of diameter D_t that moves eccentrically (e) to the axis of the hole having diameter D_h in a helical trajectory to remove the material. The advantage of the process is in terms of its versatility. A single end mill of a particular diameter can be used to process any larger holes, unlike the conventional drilling process, where the

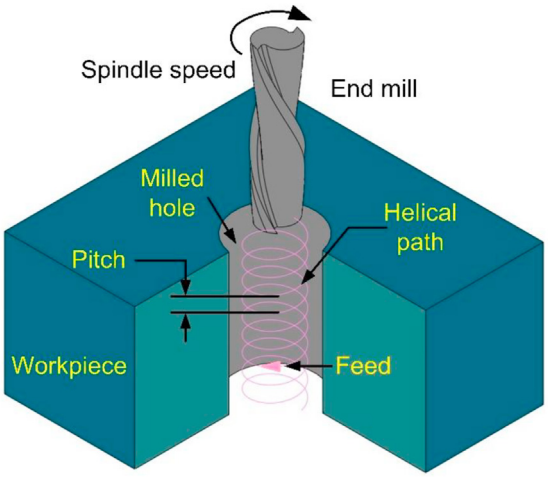

Fig. 1. Helical hole milling process.

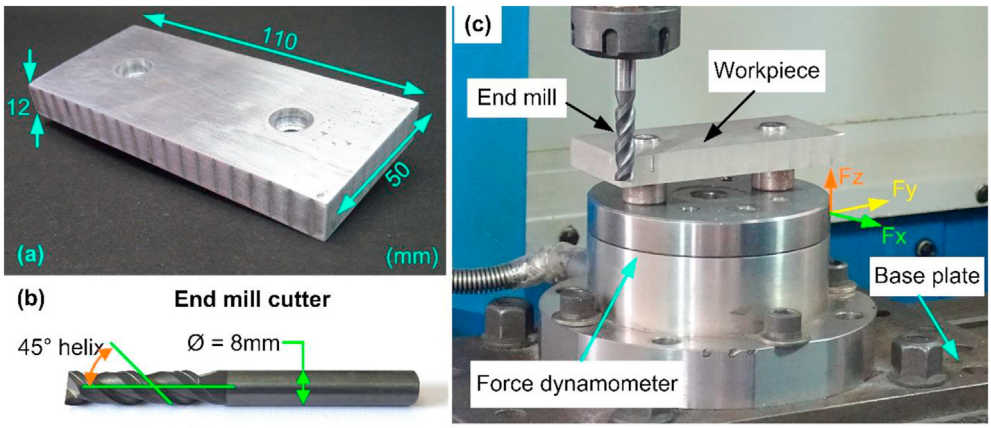

Fig. 2. (a) AZ31 magnesium alloy workpiece, (b) carbide end mill, (c) experimental set.

diameter of the drill bit should closely match the diameter of the hole being drilled. As a result, the helical hole milling process helps in reducing the tool inventory.

Iyer et al. [26] carried out a comparison study to evaluate the tool wear during hard drilling and helical milling of AISI D2 tool steel. Hard drilling under dry cutting conditions resulted in accelerated tool wear and rapid failure of the tool. However, hole processing using helical milling provided favorable results as it helped in lowering the tool wear rate and surface errors. On similar lines, Li et al. [27] examined tool wear evolution and hole surface quality in dry helical milling of Ti–6Al–4V titanium alloy. The experimental investigation evidenced the capability of helical milling to generate superior quality holes. Wang et al. [28] evaluated the drilling and helical milling process by considering the tool wear and surface roughness. The magnitude of the axial force measured during helical milling was significantly lower as compared to the drilling process. The process demonstrated its superiority by generating high-quality holes and controlled tool wear. Sun et al. [29] analyzed the microstructural behavior of the material after conducting the drilling and helical milling operations. The cutting-induced plastic deformation was less severe, and microstructural changes were marginal due to the intermittent cutting. Akula et al. [30] appraised the machinability of Ti6Al4V titanium alloy during drilling and helical milling. Helical milling produced discontinuous powdery chips, lowering the contact friction, machining temperature, and forces. The intermittent contact also aided in improving the surface finish. Festas et al. [31] evaluated the surface roughness, geometric accuracy, and chip formation mechanism in helical milling of Ti–6Al–4V and Ti–6Al–7Nb titanium alloys. Compared with the drilling process, the roughness values obtained during helical milling were considerably lower, making helical milling a better choice for processing holes in difficult-to-machine titanium alloys. Alvim et al. [32] also evaluated the machinability of AISI H13 hardened steel, considering the surface quality, circularity, and productivity. The experiments were conducted using cutting speed, axial feed per tooth, and tangential feed per tooth as control variables. Attainment of competitive levels of surface finish and hole dimensional accuracy was possible using the helical milling process. Bolar et al. [33] analyzed the capability of helical milling by considering the cutting temperature and the risk of chip ignition. The helical milling process parameters influenced the cutting temperature. However, the cutting temperature magnitude was lower as compared to the drilling process. The helical milling process produced powdery chips, and the morphological evaluation of the chips showed the presence of lamellar structures. However, no burn marks were noted on the chip surface, even at higher machining temperatures indicating a low probability of chip ignition.

The applicability of the helical milling process has also been extended to composite materials. The performance of helical milling was compared against conventional drilling for machining carbon fiber reinforced plastics (CFRP)/titanium stack by Denkena et al. [34]. The lower magnitude of cutting forces observed during the helical milling process helped improve the surface finish and dimensional accuracy. There was also a considerable reduction in the size of the exit burrs due to decreased cutting forces and temperature. Abidi et al. [35] investigated the effect of process variables viz., hole diameter, orbital feed speed, and cutting speed on delamination defect and surface roughness during helical milling of CFRP. Surface roughness was highly affected by orbital feed speed, while the hole diameter strongly influenced the delamination factor at hole entry and exit. The quality of the holes processed using helical milling in CFRP/titanium laminated structures was also investigated [36]. According to the results, titanium had little influence on the surface quality and cutting force; however, it significantly impacted the subsurface quality and cutting temperature. The high temperature lowered the resin's adhesive properties, leading to severe subsurface damage. Ben Wang et al. [37] studied the influence of drilling and helical milling on the geometric accuracy of holes made in a CFRP/Titanium laminated structure. Hole drilling in the metal layer resulted in over-cut during conventional drilling. The roundness error was also higher in the drilled holes due to CFRP material tearing. Helically milled holes produced geometrically accurate holes without any damage. Ben Wang et al. [38] studied the influence of cutting temperature on hole damage in CFRP/Titanium stacks under helical milling. It was noted that the rise in cutting temperature deteriorated the performance of the CFRP due to the resin degradation. Maximum temperature-induced damage was observed near the hole surface. Bolar et al. [39] studied the machinability of carbon fiber aluminum laminates (CARALL). The evaluation was undertaken by comparing the burr size, machining temperature, and forces. Benefits of helical milling included the lower magnitude of machining temperature and forces, coupled with smaller size burrs.

Table 1
Levels of process variables for experimentation.

Milling parameters	Level 1	Level 2	Level 3
Spindle speed (r/min)	2000	4000	6000
Tangential feed (mm/z)	0.02	0.06	0.1
Axial pitch (mm/rev)	0.1	0.3	0.5

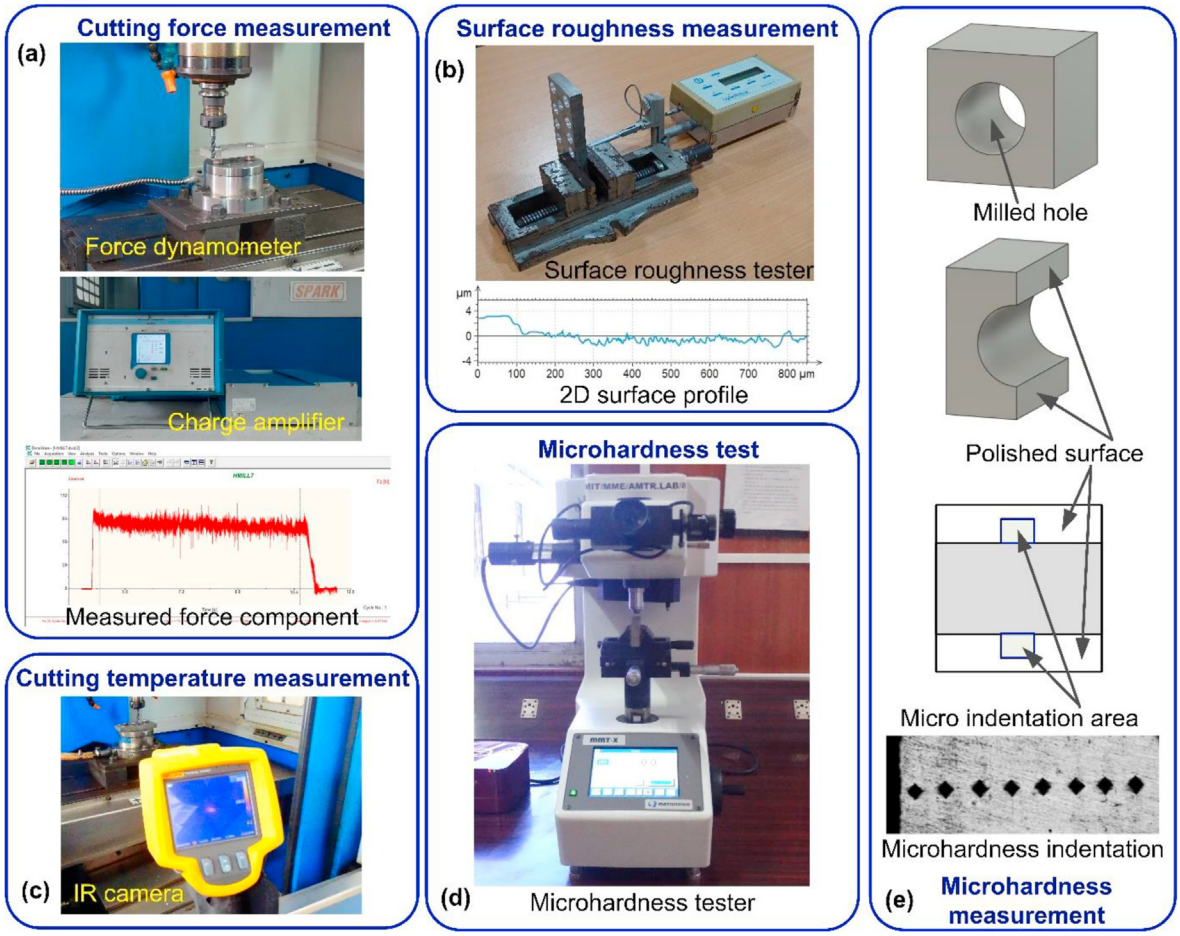

Fig. 3. (a) Force measurement, (b) surface roughness measurement, (c) machining temperature measurement, (d) microhardness test, (e) microhardness measurement.

Table 2
Designed experimental array and performance parameters.

Run	n_s (rev/min)	f_z (mm/z)	a_p (mm/rev)	F_t (N)	F_r (N)	R_a (μm)	MH_{max} (HV)
1	2000	0.02	0.5	48.41	61.09	0.59	84.9
2	4000	0.02	0.5	43.76	55.01	0.35	73.3
3	2000	0.06	0.3	54.51	44.26	0.89	84.3
4	4000	0.06	0.3	49.5	38.62	0.64	75.3
5	2000	0.1	0.5	65.83	53.1	0.95	95.5
6	6000	0.02	0.5	36.51	45.8	0.22	65.2
7	4000	0.02	0.3	35.2	48.3	0.49	71.6
8	4000	0.1	0.5	60.95	47.23	0.78	83.2
9	6000	0.1	0.5	58.06	41.81	0.41	76.3
10	2000	0.06	0.1	22.02	36.55	1.11	80.7
11	2000	0.02	0.1	17.81	42.2	0.93	75.3
12	2000	0.1	0.1	23.48	30.8	1.19	82.1
13	4000	0.02	0.1	15.56	38.46	0.55	65.2
14	6000	0.02	0.1	14.94	35.39	0.71	58.9
15	4000	0.1	0.3	55.62	36.92	0.71	78.2
16	6000	0.02	0.3	32.02	39.07	0.44	62.1
17	2000	0.1	0.3	59.44	40.35	1.03	87.6
18	4000	0.06	0.5	55.18	48.76	0.41	79.1
19	6000	0.06	0.1	17.79	24.68	0.61	62.6
20	4000	0.06	0.1	18.06	34.48	0.73	73.9
21	6000	0.06	0.5	53.59	43.93	0.34	69.8
22	2000	0.06	0.5	58.13	54.41	0.69	88.6
23	2000	0.02	0.3	37.75	50.39	0.75	79.1
24	6000	0.1	0.3	53.06	32.86	0.53	69.7
25	6000	0.06	0.3	47.34	36.15	0.41	66.4
26	6000	0.1	0.1	17.04	23.86	0.79	67.3
27	4000	0.1	0.1	22.23	28.29	0.85	78.4

Table 3
AVOVA analysis for thrust force.

Source	Sum of Squares	df	Mean Square	*F*-value	*P*-Value	Remarks
Model	7513.05	9	834.78	109.38	<0.0001	Significant
n_s	180.56	1	180.56	23.66	0.0001	Significant
f_t	993.84	1	993.84	130.22	<0.0001	Significant
a_p	5391.03	1	5391.03	706.37	<0.0001	Significant
$n_s.f_t$	0.0007	1	0.0007	0.0001	0.9926	Insignificant
$n_s.a_p$	9.52	1	9.52	1.25	0.2795	Insignificant
$f_t.a_p$	145.05	1	145.05	19.00	0.0004	Significant
n_s^2	0.5787	1	0.5787	0.0758	0.7864	Insignificant
f_t^2	55.07	1	55.07	7.22	0.0156	Significant
a_p^2	737.41	1	737.41	96.62	<0.0001	Significant
Residual	129.74	17	7.63			
Cor Total	7642.80	26		984.42		

The literature reports exclusive studies on hole drilling in magnesium alloys. As noted, several problems persist while drilling holes in magnesium alloys. Therefore, exploring alternatives that can sustainably help process quality holes has become vital. In the recent past helical milling has acquired prominence for hole processing in metallic alloys and composites. However, hole-making in magnesium alloys using helical milling remains relatively unexplored. The lack of credible knowledge on the cutting forces developed and the surface quality generated during helical milling warrants a thorough investigation. Therefore, an attempt was made to investigate the dry helical milling of AZ31 magnesium alloy. The impact of spindle speed, axial pitch, and tangential feed on thrust force, radial force, surface roughness, and microhardness was evaluated. Exhaustive experiments were carried out, and the response surface method (RSM) was applied to model the empirical equations for predicting the responses, including surface roughness, thrust force, and radial force. The contribution of process parameters to the measured responses was examined using analysis of variance (ANOVA). In addition, empirical equations for predicting the responses were derived using regression analysis. The results of the study displayed the positive impact of helical milling on thrust force, radial force, surface roughness, and microhardness, even under dry machining conditions.

2. Experimental details

The experimental investigation was carried out on AZ31 magnesium alloy produced by hot rolling process. The commercially procured plate was sized into samples of desired dimensions (size 110 × 50 × 12 mm^3) using the wire electric discharge machining (WEDM) process, as shown in Fig. 2(a). Uncoated carbide end mills shown in Fig. 2(b) were used to process holes of 12 mm diameter. All the hole milling experiments were performed on a three-axis CNC vertical machining center (*AMC Spark*). The setup used to perform the experiments is shown in Fig. 2(c).

There is limited research on helical hole milling of lightweight structural materials. Within the domain of lightweight structural materials, the majority of the literature deals with the machining of titanium [30,31] and aluminum alloys [40,41]. Therefore, process parameters and their levels for hole milling of magnesium alloys were determined by considering the machine tool constraints and cutting tool constraints. For example, the spindle speed was selected based on the machine tool limitation. The experiments were performed on a vertical machine center (VMC) with a maximum spindle speed of 8000 rev/min. Therefore, the maximum level of spindle speed for the experiments was restricted to 75% of the maximum machine spindle speed. The difference in the process kinematics of helical milling makes it slower compared to conventional drilling. Therefore, the axial pitch and tangential feed levels were determined considering the productivity level. Screening experiments were carried out using helical milling and traditional drilling processes by maintaining a constant productivity level (machining time). Lower cutting forces and comparatively good surface finish were reported during helical milling even when the productivity levels (machining time) were comparable with the conventional drilling process. Additional details pertaining to the pilot study can be accessed from the literature [42]. Based on the outcome, helical hole milling experiments were planned by considering three control factors, spindle speed, tangential feed, and axial pitch, at three levels (see Table 1). A Taguchi L27

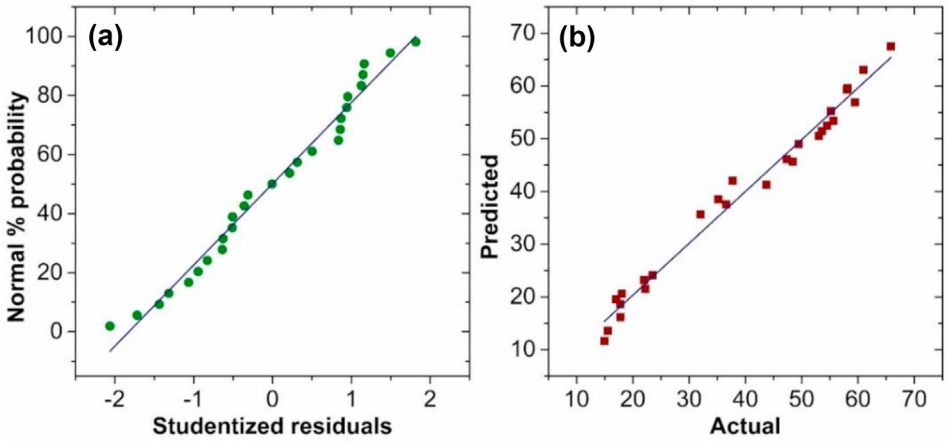

Fig. 4. (a) Normal probability residual plot, (b) predicted versus actual plot for thrust force.

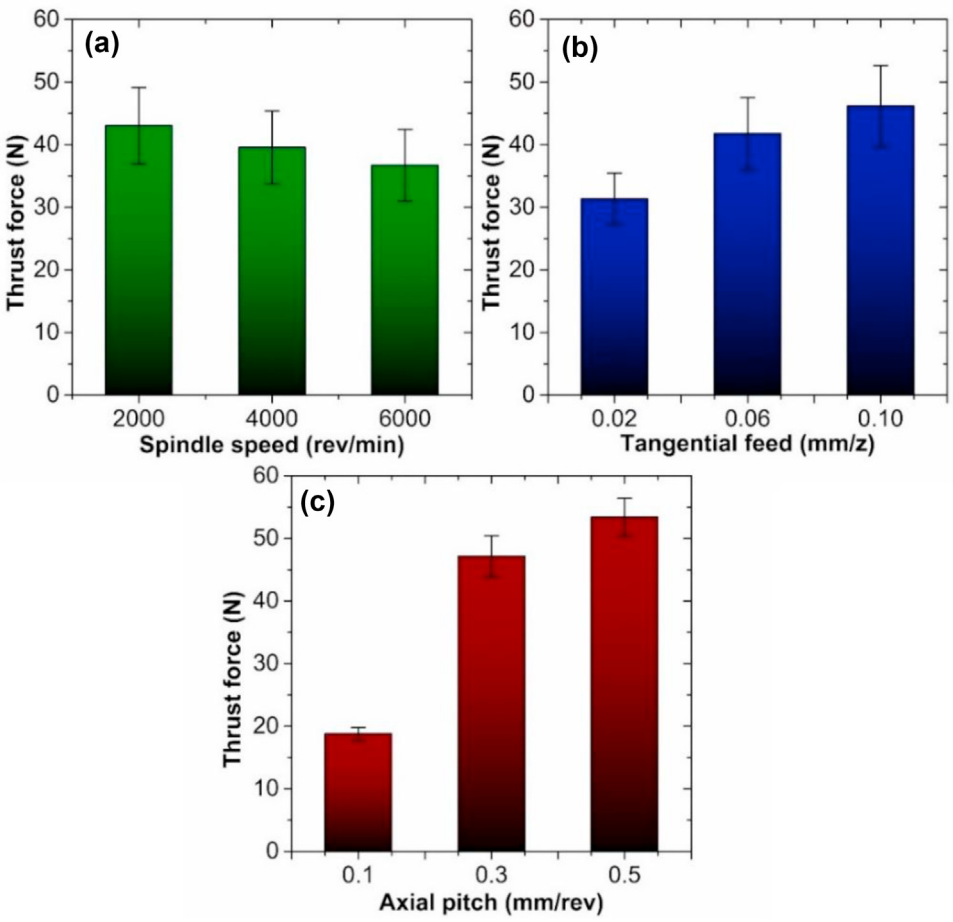

Fig. 5. Thrust force variation with (a) spindle speed, (b) tangential feed, (c) axial pitch.

orthogonal array (OA) was used to design the experiments, and a total of 27 experiments were performed. The Response Surface Method (RSM) was used to relate the performance measure, and the selected process variables and mathematical models were developed. The adequacy of the developed models and the influence of helical milling process variables was established using statistical Analysis of Variance (ANOVA).

Cutting forces were measured online by a dynamometer (Kistler 9272B) (see Fig. 3(a)) and conditioned using a charge amplifier (Kistler 5070A). DynoWare 2825A software was utilized to visualize the force data graphically. Force signals were recorded for 50 s, and the sampling rate was fixed at 4000 Hz/Channel. Offline surface roughness was performed using a portable roughness gauge (*Surtronic 3+*) according to ISO 4287. The study was carried out considering the arithmetic average (R_a). The surface roughness tester has a stylus made of diamond material and has a tip radius of 5 μm. A 2CR type filter was chosen for surface texture analysis. The cut-off length was set as 0.8 mm, and the traverse length of 4 mm was maintained. Surface roughness measurements were carried out along the axial pitch direction. The measurements were made at three angularly equidistant points, as shown in Fig. 3(b), and the average of the readings was considered.

Fig. 3(c) displays the machining temperature measurement setup during helical milling. An infrared (IR) thermal imager (*Fluke Ti32*) with a measurement range of −20 to 600 °C and accuracy of ±2 °C was used. When using the IR imagining technique, the emissivity of the materials plays a vital role in accurately measuring the temperature data. For the present study, the magnesium specimen was placed on a hot plate, and the temperature was varied from room temperature to 100 °C. The surface temperature of a specific spot was measured and monitored using the thermocouple and the IR camera. The images were captured by positioning the imager at a distance of 0.1 m from the workpiece. During the calibration, thermal emissivity for the material was found to be 0.18. Accordingly, an emissivity of 0.18 was used in the study. Vickers's test was performed to evaluate the microhardness of the machined holes using Vicker's hardness tester (*OmniTech*), as illustrated in Fig. 3(d). The milled holes were sectioned using a wire electric discharge machine (WEDM). A schematic of a sectioned cut hole is shown in Fig. 3(e). The sectioned specimens were polished manually using SiC grit papers ranging from 600 to 1200 grit size. Diamond polishing was employed to mirror finish the semi-polished samples. The micro-indentations were made along the hole radial direction using a diamond-shaped indenter under 100 g load and a dwell time of 15 s. The first microhardness indent was made at a distance of 25 μm from the milled hole surface into the bulk sample specimen along the radial direction. Subsequent indentations were made at a distance of 50 μm from the previous indentation, as shown in Fig. 3(e).

3. Results and discussion

In the present study, the milling forces and surface integrity observed during the helical milling were systematically evaluated. Table 2 shows the experimental array with measured average response values.

3.1. Analysis of thrust force

The axial force component (F_t) is considered a vital performance measure since it influences the hole surface quality and burr formation. For this reason, the thrust force is critically examined using AVOVA. The ANOVA results are shown in Table 3. *F*-value of 109.38 asserts the significance of the developed model. *P*-value < 0.05 indicates the significance of the model terms. Considering the thrust force, the model terms n_s, f_t, a_p, f_t. a_p, f_t^2, and a_p^2 are reported as significant. *R*-Squared value of 0.983 for the thrust force model indicates a very good fit. Further, excellent agreement between the adjusted *R*-Squared (= 0.974) and predicted R-Squared (= 0.9546) shows that the model is satisfactory. In addition, an adequate precision value of 33.2 confirms the competence of the model.

A normal plot of residuals for the thrust force is shown in Fig. 4(a). The residuals follow a normal distribution pattern around the straight line, verifying the normal distribution of errors. Fig. 4(b) portrays the distribution of actual and predicted values of thrust force. A closely packed distribution of the values indicates a good degree of fit and an accurate prediction capability of the response model.

Furthermore, a second-order mathematical model of thrust force (F_t) is formulated. After eliminating the insignificant terms, the selected model in terms of the actual values is given by:

$$F_t = -5.52843 - 0.0015841 \cdot n_s + 282.59722 \cdot f_t + 226.74722 \cdot a_p + 434.58333 \cdot f_t \cdot a_p - 1893.40278 \cdot f_t^2 - 277.15278 \cdot a_p^2 \quad (1)$$

Fig. 5(a) exhibits the impact of spindle speed on thrust force. Thrust force decreases with the increment in spindle speed from 2000 rev/min to 6000 rev/min. The average thrust force ranges from 36.7 N to 43.1 N. There is a decrease in thrust force by about 7%–8% with the spindle speed increment. The reduction in thrust force is associated with the cutting temperature. The magnitude of the machining temperature increases with the spindle speed, as evidenced by Fig. 6. At higher spindle speeds, the cutting process becomes highly adiabatic. Consequently, heat generated at the cutting zone is retained in the material, thereby increasing the machining temperature. The subsequent material softening eases the process of material shearing, thus lowering the magnitude of thrust force. Similar observations were made when milling titanium alloy [43,44] and AISI 5140 medium carbon alloy steel [45]. Moreover, there is a reduction in the interface contact area and specific cutting energy, as suggested by Koklu et al. [16]. As evidenced in Fig. 5(b), an increase in the tangential feed from 0.02 to 0.1 mm/z raises the thrust force. For the selected range of tangential feed, thrust force varies between 31.2 N and 46.2 N. The increment in the thrust force with tangential feed ranges between 10% and 25%. The results indicate that lower tangential feed is desirable for minimizing the thrust force. The variation in the thrust force with the increase in the tangential feed may be explained considering the undeformed chip geometry. According to Amir Rasti et al. [46], the magnitude of thrust force is a function of material available at the edge of the cutting tooth. The volume of material available at the cutting-edge (undeformed chip geometry) increases at a higher tangential feed. The resulting increase in the plastic deformation energy increases the magnitude of the thrust force. Fig. 5(c) presents the fluctuation of thrust force with axial pitch. The thrust force increases by 12%–60%, with the axial pitch rising from 0.1

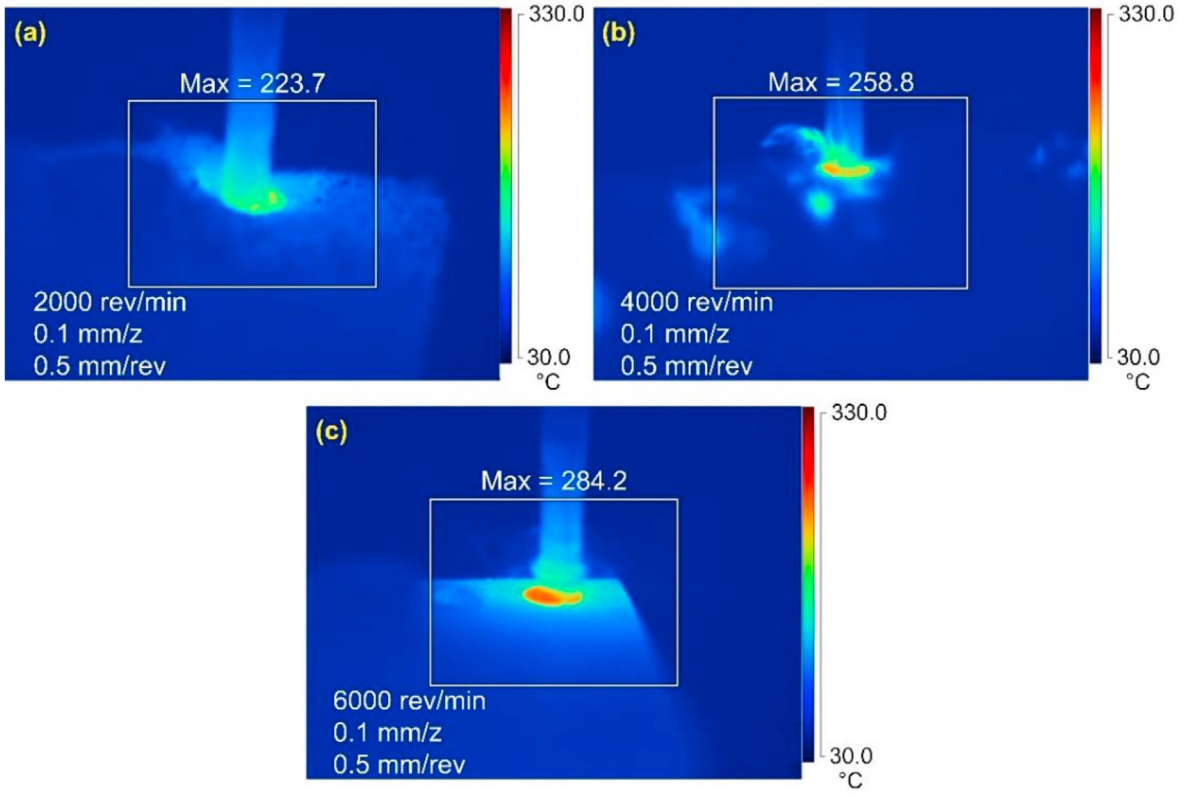

Fig. 6. Maximum machining temperature variation with spindle speed.

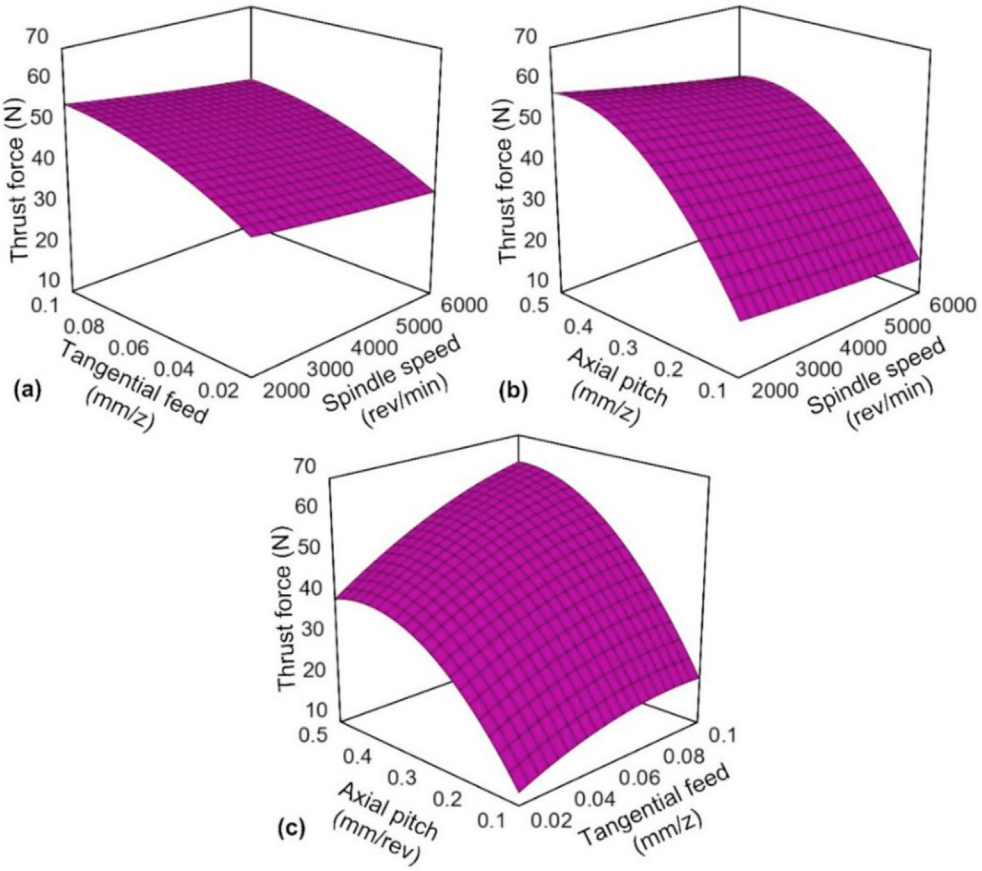

Fig. 7. Response surface for the interaction effects of (a) spindle speed and tangential feed, (b) spindle speed and axial pitch, (c) tangential feed and axial pitch.

Table 4
AVOVA analysis for radial force.

Source	Sum of Squares	df	Mean Square	*F*-value	*P*-Value	Remarks
Model	2216.91	9	246.32	119.62	<0.0001	Significant
n_s	446.01	1	446.01	216.59	<0.0001	Significant
f_t	359.92	1	359.92	174.79	<0.0001	Significant
a_p	1359.46	1	1359.46	660.18	<0.0001	Significant
$n_s.f_t$	4.94	1	4.94	2.40	0.1398	Insignificant
$n_s.a_p$	10.91	1	10.91	5.30	0.0343	Significant
$f_t.a_p$	14.83	1	14.83	7.20	0.0157	Significant
n_s^2	4.41	1	4.41	2.14	0.1614	Insignificant
f_t^2	13.75	1	13.75	6.68	0.0193	Significant
a_p^2	2.67	1	2.67	1.30	0.2705	Insignificant
Residual	35.01	17	2.06			
Cor Total	2251.92	26				

mm/rev to 0.5 mm/rev. In Ref. [47], it is reported that with the increase in the axial depth, there is a change in the length of engagement of the workpiece and the cutting tool. The increase in the engagement length increases the volume of deforming material and, consequently, the thrust force.

Fig. 7(a) depicts the interaction of control parameters, namely, tangential feed and spindle speed on thrust force. Thrust magnitude increases with the increase in tangential feed, while spindle speed demonstrates a decreasing trend. Lower thrust force can be obtained by choosing lower spindle speed and tangential feed values. Fig. 7(b) displays the interaction plot between the spindle speed and axial pitch. Both the control parameters significantly influence the thrust force, as reported in Table 3. However, the spindle speed increment showed a decreasing thrust force trend, while the thrust force showed an increasing trend with the rise in axial pitch. The effect of tangential feed combined with axial pitch is depicted in Fig. 7(c). Thrust force climbs with the simultaneous increase in axial pitch and tangential feed. Moreover, the interaction of axial pitch and tangential feed is highly influential, as seen in Table 3. Developed response surface plots illustrate that a lower magnitude of thrust force can be maintained by employing a higher spindle and lower levels of tangential feed and axial pitch.

3.2. Analysis of radial force

The radial force component (F_r) is associated with the side cutting edge of the milling cutter. A very high magnitude of radial force affects the dimensional and surface quality of the holes [29].

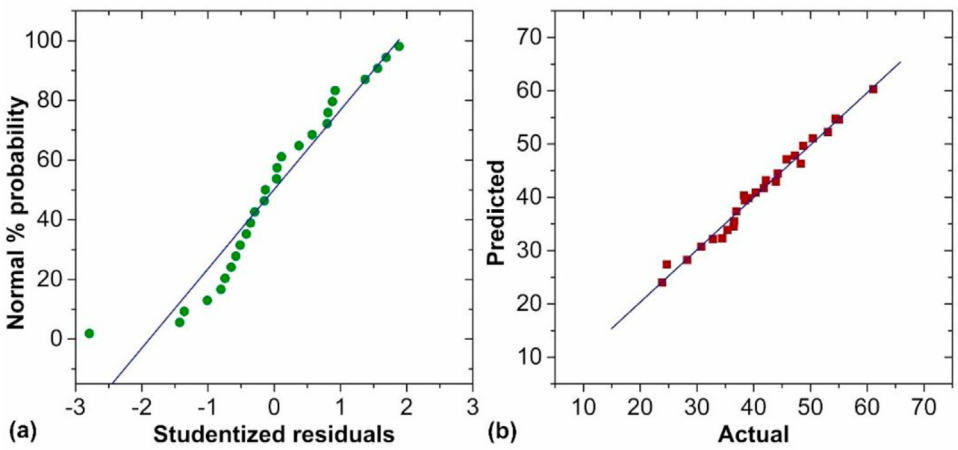

Fig. 8. (a) Normal probability residual plot, (b) predicted versus actual plot for radial force.

Hence, AVOVA was employed to evaluate the radial force. Table 4 lists the outcome of ANOVA for radial force. A high *F*-value of the model is 2216.91, which establishes the significance of the model. Model *P*-value (<0.05) also demonstrates the importance of the model. Considering the radial force, the model terms n_s, f_t, a_p, n_s. a_p, f_t. a_p and f_t^2 are found to be significant. The proposed model provides the best correlation between the response (radial force) and process parameters as the value of R-Squared is 0.9845. Close conformity of the predicted *R*-Squared (0.9621) with the adjusted *R*-Squared (0.9762) is reported.

Normal probability plots of residual for investigation of radial force are shown in Fig. 8(a). The residuals follow a normal distribution pattern along a straight line, which verifies the normality test for thrust force. Fig. 8(b) portrays the distribution of experimental and predicted radial force values. A closely packed distribution of the values indicates a good fit and excellent correlation

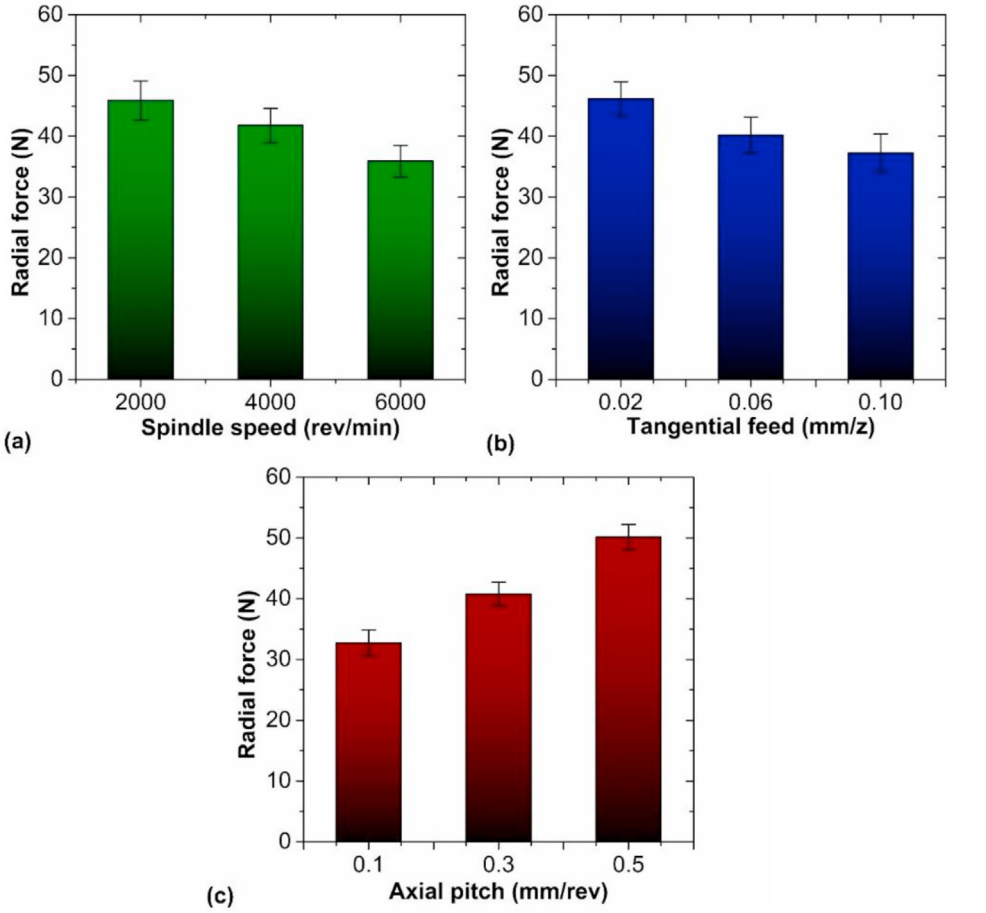

Fig. 9. Variation of radial force with (a) spindle speed, (b) tangential feed, (c) axial pitch.

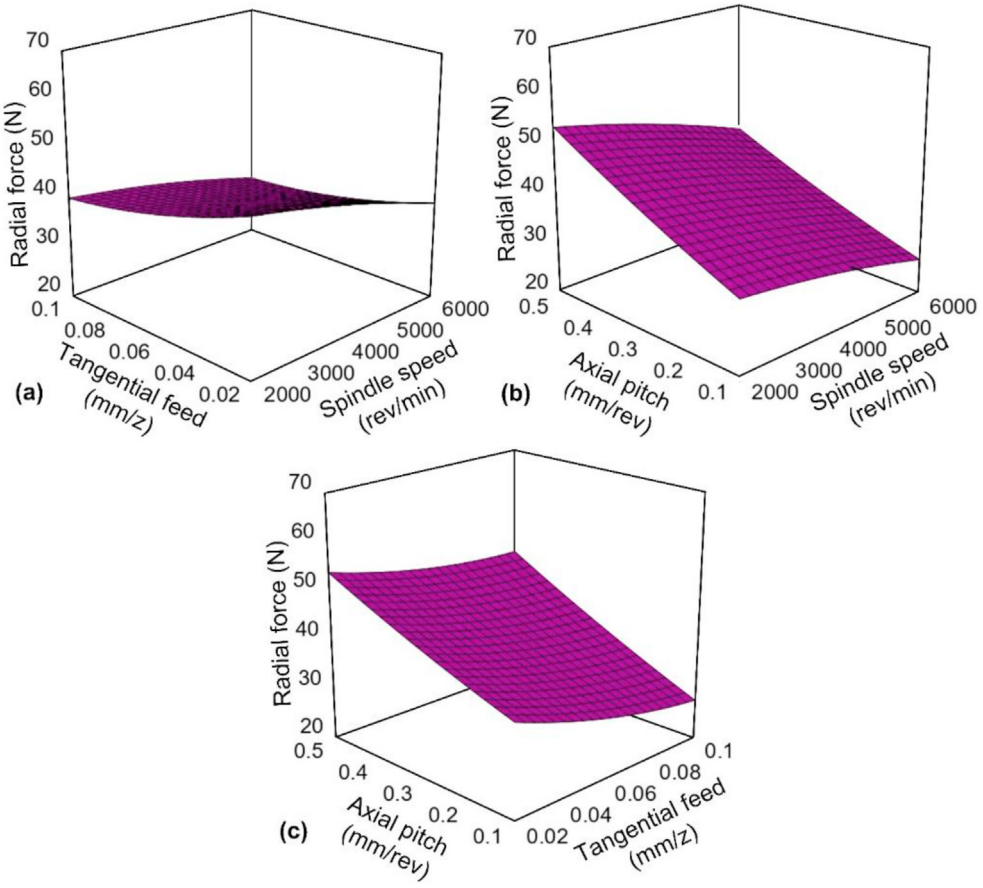

Fig. 10. Response surface for the interaction effects of (a) spindle speed and tangential feed, (b) spindle speed and axial pitch, (c) tangential feed and axial pitch on radial force.

between the predicted and experimental radial force. The second-order mathematical model of radial force is given by:

$$F_r = 28.46167 - 0.001774 \cdot n_s + 39.93750 \cdot f_t + 61.32361 \cdot a_p - 0.002383 \cdot n_s \cdot a_p - 138.95833 f_t \cdot a_p + 946.18056 \cdot f_t^2 \quad (2)$$

Fig. 9(a) displays the impact of spindle speed on the radial force. The magnitude of radial force decreases with the increase in spindle speed from 2000 rev/min to 6000 rev/min. For the three levels of spindle speed, the average radial force ranges from 36 N to 461 N. With the increase in spindle speed, there is a decrease in thrust force by about 9%–14%. Similar remarks were made by Bi et al. [48]. According to them, the reduction in the radial force magnitude at higher spindle speed is credited to the decrease in the contact area at the interface of the tool-workpiece. Additionally, the rise in machining temperature at higher spindle speed lowers the material yield strength and its hardness, thus the force for radial cutting of the material [49]. Fig. 9(b) shows the progress of radial force with tangential feed. The radial forces decrease as tangential feed increases from 0.02 to 0.1 mm/z. For the selected range, radial force varied between 37.2 N and 46.2 N. The radial force decreased by 7%–13% with the increase in tangential feed. According to Li et al. [50], undeformed chip height reduces as the tangential feed increases. Reduction in the undeformed chip size lowers the edge force; as a result, the radial force drops. Fig. 9(c) presents the fluctuation of radial force with axial pitch from 0.1 mm/rev to 0.5 mm/rev. The radial force varied between 32.7 N–50.1 N, an increase

Table 5
AVOVA analysis for surface roughness.

Source	Sum of Squares	df	Mean Square	*F*-value	*P*-value	Remarks
Model	1.57	9	0.1744	58.22	<0.0001	Significant
n_s	0.7647	1	0.7647	255.27	<0.0001	Significant
f_t	0.1964	1	0.1964	65.55	<0.0001	Significant
a_p	0.4934	1	0.4934	164.69	<0.0001	Significant
$n_s.f_t$	0.0208	1	0.0208	6.95	0.0173	Significant
$n_s.a_p$	0.0027	1	0.0027	0.9013	0.3557	Insignificant
$f_t.a_p$	8.333E-06	1	8.333E-06	0.0028	0.9586	Insignificant
n_s^2	0.0888	1	0.0888	29.65	<0.0001	Significant
f_t^2	0.0024	1	0.0024	0.8012	0.3832	Insignificant
a_p^2	0.0006	1	0.0006	0.2003	0.6601	Insignificant
Residual	0.0509	17	0.0030			
Cor Total	1.62	26				

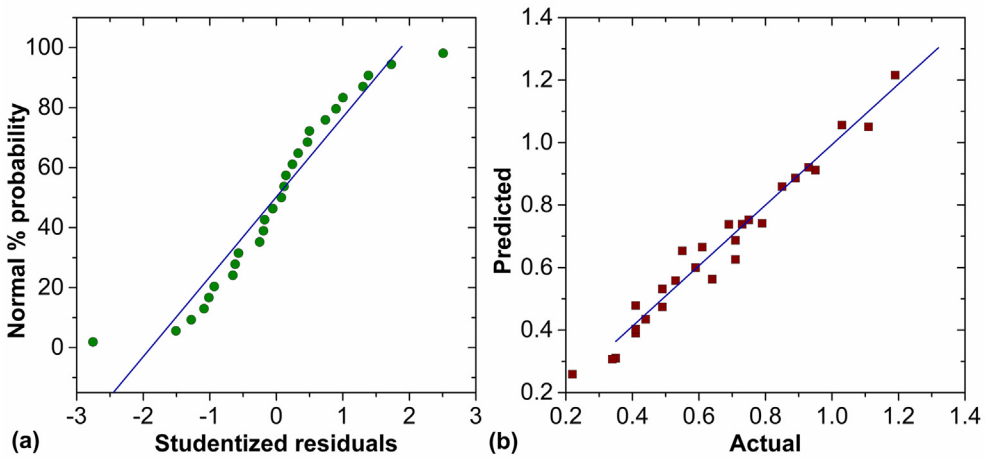

Fig. 11. (a) Normal probability residual plot, (b) predicted versus actual plot for surface roughness.

of 19%–24%. With the rise in axial pitch, tool axial feed increases. The associated increase in work-tool contact length increases the shearing energy and, thus, the radial force. Similar observations were made by Pereira et al. [41].

Fig. 10 demonstrates the 3D response plots for spindle speed, tangential feed, and axial pitch in pairs. Fig. 10(a) exhibits the interaction plot between the tangential feed and spindle speed. Both the control parameters significantly influence the radial force, as reported in Table 4. Spindle speed and tangential feed increment lower the radial force magnitude. The combined effect of spindle speed and axial pitch is depicted in Fig. 10(b). Again, the interaction of axial pitch and spindle speed is highly influential, as seen in Table 4. Lower radial force can be maintained by selecting higher levels of spindle speed while utilizing lower axial pitch. The effect of tangential feed combined with axial pitch is depicted in Fig. 10(c). The radial force decreases with the tangential feed,

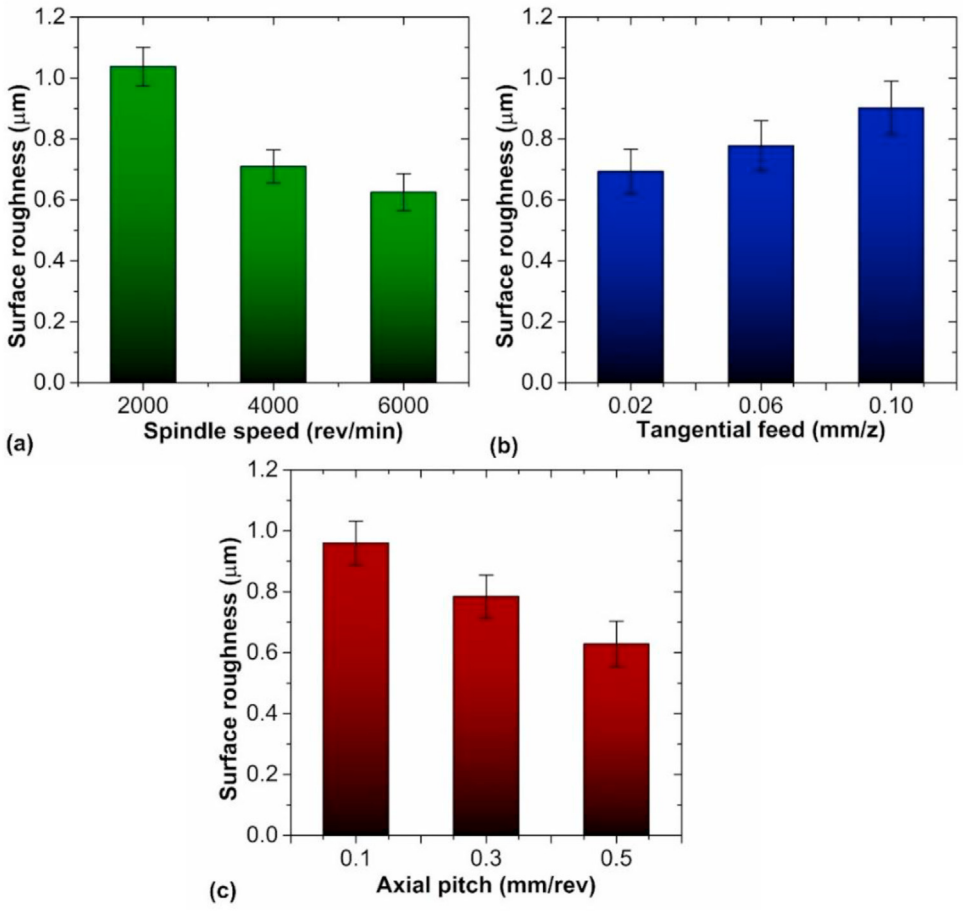

Fig. 12. Variation of surface roughness with (a) spindle speed, (b) tangential feed, (c) axial pitch.

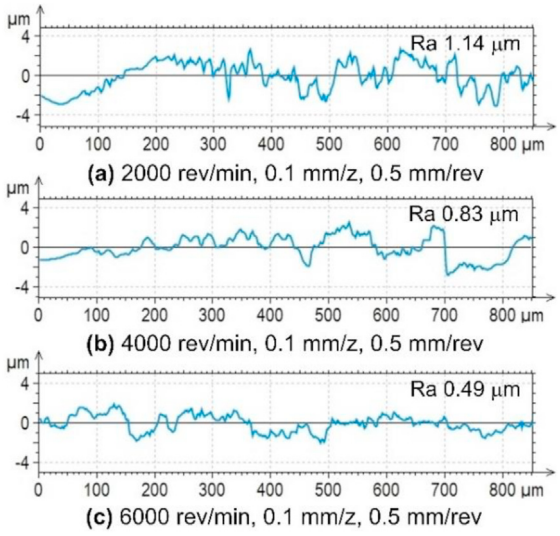

Fig. 13. 2D surface profile when machined using a spindle speed of (a) 2000 rev/min, (b) 4000 rev/min, (c) 6000 rev/min.

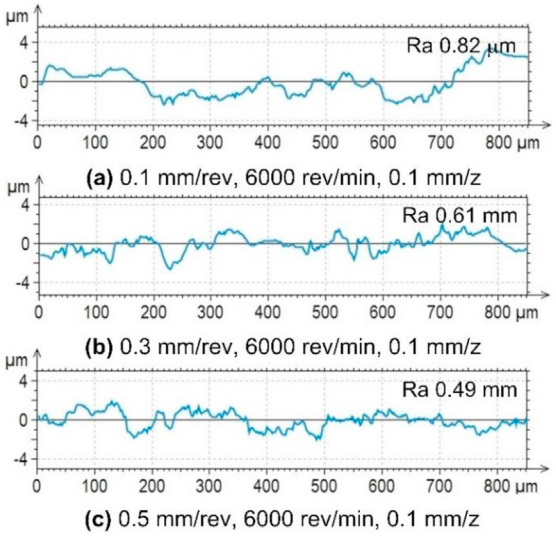

Fig. 15. 2D surface profile when machined using axial pitch of (a) 0.1 mm/rev, (b) 0.3 mm/rev, (c) 0.5 mm/rev.

although an increasing trend is exhibited with the increasing axial pitch.

3.3. Analysis of surface roughness

Surface roughness influences the tribological behavior of the machined components [51]. Moreover, a higher magnitude of surface roughness can serve as a site for stress concentration and microcrack initiation [52,53]. Considering the significance of the performance measure, ANOVA was executed to identify the influential process parameters affecting the surface roughness. Table 5 presents the ANOVA for surface roughness. A *F*-value of 58.22 for the model demonstrates the significance of the developed model. *P*-value lower than 0.05 proves that all three process variables are important and significant. In addition, the model terms n_s. f_t, and n_s^2 are significant. *R*-Squared of 0.9686 indicates the best possible correlation between surface roughness and process variables. The predicted *R*-Squared of 0.9158 shows acceptable conformity with the adjusted *R*-Squared (0.9519).

The regression model for surface roughness after the removal of non-significant terms is given by:

$$R_a = 1.57556 - 0.000315 \cdot n_s + 4.69444 \cdot f_t - 0.827778 \cdot a_p - 0.000521 \cdot n_s \cdot f_t + 3.04167 \cdot 10^{-8} \cdot n_s^2 \quad (3)$$

Fig. 11(a) details the normal probability plot demonstrating the normal distribution of the residuals. Moreover, the close distribution of the predicted and experimental values along a straight line shows the remarkable prediction capability of the developed model (see Fig. 11(b)).

Fig. 12(a) displays the surface roughness deviation with spindle speed. Surface roughness decreases as the spindle speeds increase. At 2000 rev/min spindle speed, the average surface roughness of about 0.91 μm is measured. With the increment in spindle speed to 4000 rev/min and 6000 rev/min, the magnitude of surface roughness reduced to 0.58 μm and 0.49 μm, respectively. The reduction in the surface roughness with spindle speed can be verified using the 2D surface profile shown in Fig. 13. A drop of 13%–36% is reported as the spindle speed increases. The reduction is attributed to the decrease in the machining forces. An increase in machining temperature at higher spindle speeds lowers the material yield stress, thereby facilitating the reduction in friction and machining forces. This helps improve the process stability and the surface finish [47,54]. Similar observations were made by Usca et al. [55], where there was an improvement in the surface finish due to the reduction in cutting forces at higher cutting speeds. Moreover, the reduced contact time between the chip and the newly machined surface at higher spindle speeds prevents the chip from curling and surface damage [56]. Fig. 12(b) illustrates the effect of increasing the tangential feed on surface roughness. Fig. 14 shows the 2D profile of the hole surface for various tangential feeds. As evidenced, the surface roughness increases by about 13%–16% as tangential feed increases. For the selected range of feed per tooth, the surface roughness varies between 0.56 μm and 0.77 μm. The increase in the surface roughness with the feed value is attributed to the undeformed chip thickness. According to Amini et al. [57], the undeformed chip thickness increases as the feed value increases. This causes the milling force to increase drastically.

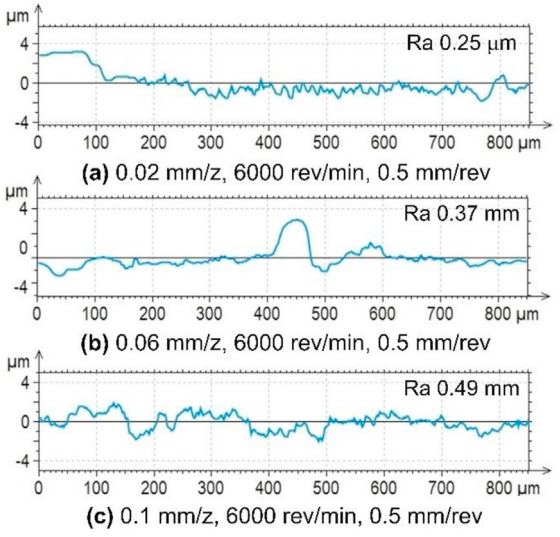

Fig. 14. 2D surface profile when machined using tangential feed of (a) 0.02 mm/z, (b) 0.06 mm/z, (c) 0.1 mm/z.

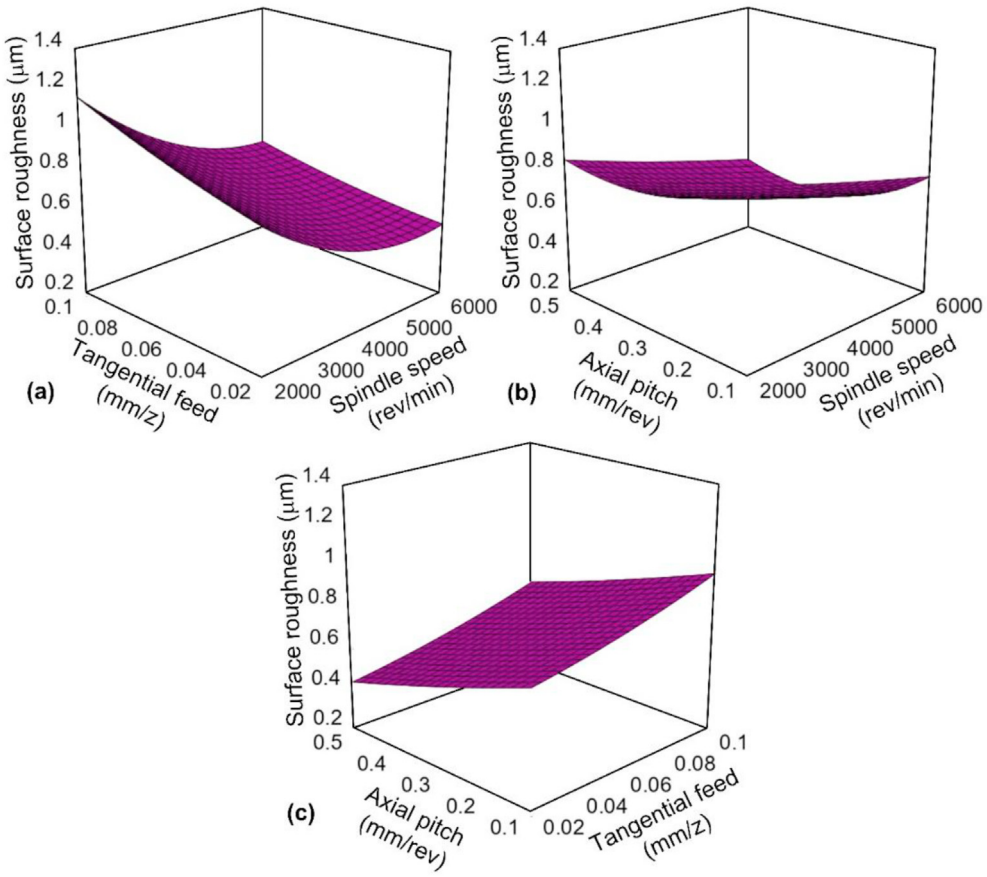

Fig. 16. Response surface for the interaction effects of (a) spindle speed and tangential feed, (b) spindle speed and axial pitch, (c) tangential feed and axial pitch for surface roughness.

Subsequently, the system stability decreases, thereby increasing the surface roughness. Similar remarks were made by Rasti et al. [46], who, based on their study, concluded that the integrity of the machined surface depends on the undeformed chip thickness and cutting forces.

Fig. 12(c) explains the influence of axial pitch on surface roughness. A decreasing trend is noticed as the axial pitch increases to 0.5 mm/rev (see Fig. 15). The average surface roughness is 0.83 μm when the axial pitch is maintained at 0.1 mm/rev. With the increase in axial pitch to 0.3 mm/rev and 0.5 mm/rev, surface roughness reduces to 0.65 μm and 0.49 μm, respectively. An average 21%–25% reduction in the average surface roughness is noted as the axial pitch was increased. The poor surface finish at a lower axial pitch is ascribed to chip thickness. Due to the smaller uncut chip thickness, the probability of material ploughing at the tool tip increases. Material ploughing results in non-uniform plastic flow and poor surface finish [58]. According to Ref. [54], ploughing forces appear at lower depths of cut and feed rates. The smaller undeformed chip thickness associated with lower feed and depth of cut results in non-uniform plastic flow, thereby deteriorating the surface quality. However, at a higher axial pitch, the probability of material plowing reduces due to the increase in tool-work engagement length, thereby improving the surface quality.

Fig. 16(a) presents the interaction effect between tangential feed and spindle speed on surface roughness. An increasing trend is observed with the tangential feed, whilst the increase in spindle speed shows a reducing trend. Response surface plots depict that a superior surface finish can be achieved by combining lower tangential feed with high spindle speeds. Further, the interaction of axial pitch with spindle speed and axial pitch and tangential feed showed a contradictory trend, as shown in Fig. 16(b) and (c), respectively. However, the interaction effects have little influence on surface roughness, as seen in Table 5.

3.4. Analysis of microhardness

The hardness of the machined holes was investigated by comparing the microhardness of the as-received sample. The measured average microhardness of the as-received was 51.4 HV.

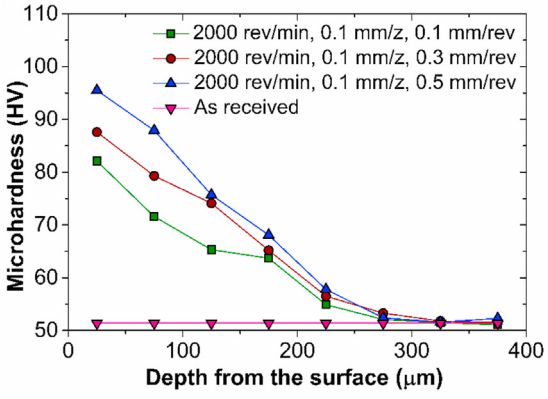

Fig. 17. Typical microhardness profile from helical milling.

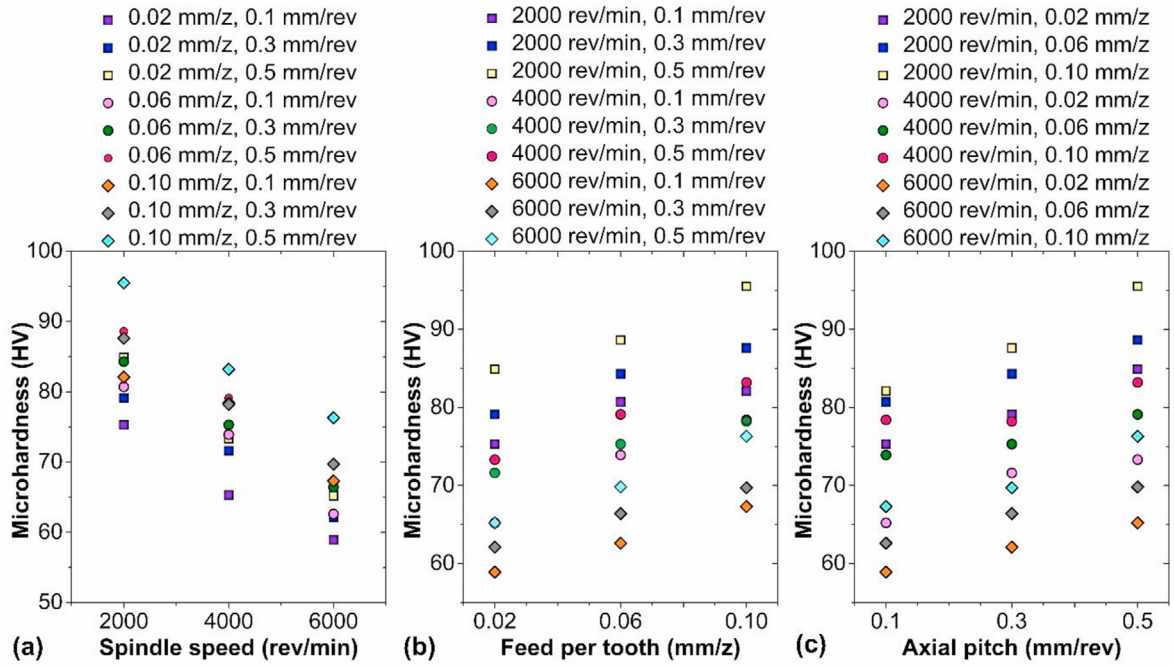

Fig. 18. Process parameters vs. maximum microhardness during helical milling.

Fig. 17 shows the microhardness distribution along with the milled surface depth for different axial pitch values (0.1–0.5 mm/rev). The microhardness closer to the machined surface was observed to be higher than the hardness at the subsurface. The increased hardness is associated with the severe work-hardening induced by plastic deformation at the work surface. However, along the subsurface, when the distance of 275 μm was reached, the microhardness gradually reduced and reached the bulk hardness due to the reduction in plastic deformation at the subsurface.

Fig. 18(a) illustrates maximum hardness behaviour with the spindle speed. The maximum microhardness decreases with increasing spindle speed. With the rise in spindle speed to 4000 rev/min, microhardness reduces by about 4.5%–13.7%. Further rise in the speed to 6000 rev/min lowers the hardness by about 18%–23.2%. The reduction in the microhardness is ascribed to the thermal softening due to the heat generated as the material is plastically deformed. The increased machining temperature lowers the material flow stress, thereby reducing the dislocation density and the hardness. The results auger well with the observations made by Shi et al. [59] when machining magnesium alloy. The hardness variation with tangential feed is shown in Fig. 18(b). The microhardness of the helically milled hole surface increases as the tangential feed increases. An increase in the tangential feed to 0.1 mm/z increases the hardness by about 4.2%–11.8%. The hardness value increased by about 8.3%–16.8% as the feed increased to 0.15 mm/z. As discussed, the cutting load, as well as the plastic deformation, increases. The resulting strain hardening at higher strain rates increases the hardness of the milled material. Similar to the spindle speed, the magnitude of the machining temperature rises as the tangential feed increases. However, microhardness variation showed an opposing trend for the tangential feed. This indicates that the machining temperature associated with thermal softening has a lower influence on microhardness, while the work hardening effect related to plastic deformation is a more dominant phenomenon affecting microhardness. The results of the present study agree well with the observations made by Rasti et al. [46] during the helical milling of AISI 4340 steel. They noted that the microhardness increased with the feed rate due to excessive work hardening.

The variation of maximum microhardness with the axial pitch is shown in Fig. 18(c). The magnitude of hardness increased as the axial pitch increased. As the axial pitch increased to 1.5 mm/rev, the hardness magnitude increased by about 0.3%–8.9%. With the further rise in axial pitch to 2.5 mm/rev, the hardness value increases by about 5.8%–14%. Akin to feed, an increase in axial pitch increases the plastic strain and, thus the microhardness.

4. Conclusions

The presented study investigated the machining characteristics of structural AZ31 magnesium alloy during the helical hole milling process. The experimental investigation was carried out to process holes with high quality and upgrade the database on machining characteristics of AZ31 magnesium alloy during the helical hole milling process. The impact of spindle speed, tangential feed, and axial pitch on thrust force, radial force, surface roughness, and microhardness was examined. The salient conclusions are summarized as follows:

- The average thrust force variation with the spindle speed ranged from 36.7 N to 43.1 N. When higher spindle speeds were chosen, a 7%–8% decrease in thrust force was observed. The reduction in the thrust force at higher spindle speeds is attributed to increased cutting temperature and subsequent material softening and flow stress reduction.
- Thrust force increased with the increase in tangential feed and axial pitch by about 10%–25% and 12%–60%, respectively. The increased thrust force at higher tangential feed and axial pitch is the function of material volume available at the cutting-edge (undeformed chip geometry) and length of chip-tool engagement.
- Radial forces generated in helical milling ranged between 36 N and 45.9 N for the spindle speed, and the magnitude of radial force decreased as higher spindle speeds were employed. The

reduction in the radial force magnitude at higher spindle speed is credited to the decrease in the contact area at the interface of the tool-workpiece.

- The radial forces varied between 37.2 N–46.2 N and 18.8 N–53.4 N depending on the level of tangential feed and axial pitch. The radial force decreased with the increase in tangential feed, while an opposite trend was witnessed as the axial pitch increased. The smaller magnitude of radial force at higher tangential feeds resulted from the reduction in the undeformed chip size at the cutting edge, while the increased length of work-tool contact at higher axial pitch increased the shearing energy and, thus, the radial force.
- The reduction in surface roughness at higher spindle speeds is attributed to the lower friction and machining forces. The decrease in contact time at higher speeds also improved the surface finish. Moreover, the reduction in ploughing forces at high axial pitch also helped in improving the quality of the processed surface. However, increased undeformed chip thickness at higher feeds increased the milling forces and thus lowered the system stability and deteriorated the surface quality.
- All three process variables exerted a crucial influence on surface roughness. Spindle speed was the most significant contributor (48.6%), followed by axial pitch (31.4%) and tangential feed (12.5%). Minimum surface roughness can be achieved by maintaining the spindle speed at 6000 rev/min, tangential feed at 0.02 mm/z, and axial pitch at 0.5 mm/rev.
- An increase in surface hardness is associated with the severe work-hardening induced by plastic deformation. The microhardness gradually reached the bulk hardness at a distance of 275 μm as a result of the reduction in plastic deformation at the subsurface. An increase in the spindle speed ensued in a decrease in microhardness by about 4%–23%. However, the tangential feed and axial pitch rise triggered a rise in the hardness magnitude by about 4.2%–16.8% and 0.3%–14%, respectively.

The experimental results reveal that helical milling can produce smaller thrust and radial forces and better surface integrity. Based on the advantages, helical milling can be considered a suitable alternative for processing holes in magnesium alloys. In the future, additional analyses can be carried out to optimize the helical milling process and also evaluate the phenomenon of tool wear and productivity improvement by considering the use of coated tools.

Funding

This research did not receive any specific grant from funding agencies in the public, commercial, or not-for-profit sectors.

Conflicts of interest

The authors declare that there is no conflicts of interest.

References

[1] N. Deswal, R. Kant, Experimental investigation on magnesium AZ31B alloy during ultrasonic vibration assisted turning process, Mater. Manuf. Process. (2022) 1–7, https://doi.org/10.1080/10426914.2022.2039701.
[2] N. Sezer, Z. Evis, S.M. Kayhan, A. Tahmasebifar, M. Koç, Review of magnesium-based biomaterials and their applications, J. Magnes. Alloys 6 (2018) 23–43, https://doi.org/10.1016/j.jma.2018.02.003.
[3] B.L. Mordike, T. Ebert, Magnesium: properties-applications-potential, Mater. Sci. Eng. A 302 (2001) 37–45, https://doi.org/10.1016/S0921-5093(00)01351-4.
[4] K.Z. Chong, T.S. Shih, Optimizing drilling conditions for AZ61A magnesium alloy, Mater. Trans. 43 (2002) 2148–2156, https://doi.org/10.2320/matertrans.43.2148.
[5] J. Wang, Y.B. Liu, J. An, L.M. Wang, Wear mechanism map of uncoated HSS tools during drilling die-cast magnesium alloy, Wear 265 (2008) 685–691, https://doi.org/10.1016/j.wear.2007.12.009.
[6] S. Bhowmick, M.J. Lukitsch, A.T. Alpas, Dry and minimum quantity lubrication drilling of cast magnesium alloy (AM60), Int. J. Mach. Tool Manufact. 50 (2010) 444–457, https://doi.org/10.1016/j.ijmachtools.2010.02.001.
[7] F. Berzosa, B. de Agustina, E.M. Rubio, Tool selection in drilling of magnesium UNSM11917 pieces under dry and MQL conditions based on surface roughness, Procedia Eng 184 (2017) 117–127, https://doi.org/10.1016/j.proeng.2017.04.076.
[8] B. de Agustina, F. Berzosa, E.M. Rubio, M.M. Marín, Experimental study of magnesium drilling based on the surface quality, Procedia CIRP 79 (2019) 74–78, https://doi.org/10.1016/j.procir.2019.02.014.
[9] U. Koklu, S. Morkavuk, L. Urtekin, Effects of the drill flute number on drilling of a casted AZ91 magnesium alloy, Mater. Test. 61 (2019) 260–266, https://doi.org/10.3139/120.111315.
[10] B.R. Sunil, K.V. Ganesh, P. Pavan, G. Vadapalli, C. Swarnalatha, P. Swapna, G.P.K. Reddy, Effect of aluminum content on machining characteristics of AZ31 and AZ91 magnesium alloys during drilling, J. Magnes. Alloys 4 (2016) 15–21, https://doi.org/10.1016/j.jma.2015.10.003.
[11] S. Yazman, U. Köklü, L. Urtekin, S. Morkavuk, L. Gemi, Experimental study on the effects of cold chamber die casting parameters on high-speed drilling machinability of casted AZ91 alloy, J. Manuf. Process. 57 (2020) 136–152, https://doi.org/10.1016/j.jmapro.2020.05.050.
[12] E. Gariboldi, Drilling a magnesium alloy using PVD coated twist drills, J. Mater. Process. Technol. 134 (2003) 287–295, https://doi.org/10.1016/S0924-0136(02)01111-1.
[13] S. Bhowmick, A.T. Alpas, The role of diamond-like carbon coated drills on minimum quantity lubrication drilling of magnesium alloys, Surf. Coat. Technol. 205 (2011) 5302–5311, https://doi.org/10.1016/j.surfcoat.2011.05.037.
[14] F. Karaca, B. Aksakal, Effect of the TIBN coating on a HSS drill when drilling the MA8M Mg alloy, Mater. Technol. 50 (2016) 75–79, https://doi.org/10.17222/mit.2014.290.
[15] A.H. Kheireddine, A.H. Ammouri, T. Lu, I.S. Jawahir, R.F. Hamade, An FEM analysis with experimental validation to study the hardness of in-process cryogenically cooled drilled holes in Mg AZ31B, Procedia CIRP 8 (2013) 588–593, https://doi.org/10.1016/j.procir.2013.06.156.
[16] U. Koklu, H. Coban, Effect of dipped cryogenic approach on thrust force, temperature, tool wear and chip formation in drilling of AZ31 magnesium alloy, J. Mater. Res. Technol. 9 (2020) 2870–2880, https://doi.org/10.1016/j.jmrt.2020.01.038.
[17] D.T. Minh, L.T. The, N.T. Bao, Performance of Al_2O_3 nanofluids in minimum quantity lubrication in hard milling of $60Si_2Mn$ steel using cemented carbide tools, Adv. Mech. Eng. 9 (2017) 1–9, https://doi.org/10.1177/1687814017710618.
[18] R. Teimouri, S. Amini, M. Lotfi, M. Alinaghian, Sustainable drilling process of 1045 steel plates regarding minimum energy consumption and desired work quality, Int. J. Lightweight Mater. Manuf. 2 (2019) 397–406.
[19] B.T. Tai, D.A. Stephenson, R.J. Furness, A.J. Shih, Minimum quantity lubrication (MQL) in automotive powertrain machining, Procedia CIRP 14 (2014) 523–528, https://doi.org/10.1016/j.procir.2014.03.044.
[20] Y. Su, Z. Li, L. Li, J. Wang, H. Gao, G. Wang, Cutting performance of micro-textured polycrystalline diamond tool in dry cutting, J. Manuf. Process. 27 (2017) 1–7, https://doi.org/10.1016/j.jmapro.2017.03.013.
[21] S.Y. Hong, Y. Ding, W.C. Jeong, Friction and cutting forces in cryogenic machining of Ti–6Al–4V, Int. J. Mach. Tool Manufact. 41 (2001) 2271–2285, https://doi.org/10.1016/S0890-6955(01)00029-3.
[22] Y. Li, H. Chen, X. Zhang, C. Tan, Y. Ding, Renewable energy carriers: hydrogen or liquid air/nitrogen? Appl. Therm. Eng. 30 (2010) 1985–1990, https://doi.org/10.1016/j.applthermaleng.2010.04.033.
[23] S.Y. Hong, Economical and ecological cryogenic machining, Manuf. Sci. Eng. 123 (2001) 331–338, https://doi.org/10.1115/1.1315297.
[24] T.C. Yap, Roles of cryogenic cooling in turning of superalloys, ferrous metals, and viscoelastic polymers, Technologies 7 (2019) 1–10, https://doi.org/10.3390/technologies7030063.
[25] A. Iqbal, H. Suhaimi, N. He, A sustainability comparison between drilling and milling for hole-enlargement in machining of hardened steels, Mach. Sci. Technol. 23 (2019) 712–733, https://doi.org/10.1080/10910344.2019.1575409.
[26] R. Iyer, P. Koshy, E. Ng, Helical milling: an enabling technology for hard machining precision holes in AISI D2 tool steel, Int. J. Mach. Tool Manufact. 47 (2007) 205–210, https://doi.org/10.1016/j.ijmachtools.2006.04.006.
[27] H. Li, G. He, X. Qin, G. Wang, C. Lu, L. Gui, Tool wear and hole quality investigation in dry helical milling of Ti-6Al-4V alloy, Int. J. Adv. Manuf. Technol. 71 (2014) 1511–1523, https://doi.org/10.1007/s00170-013-5570-0.
[28] B. Wang, K. Chang, M. Wang, F. Zhang, Y. Zhang, Y. Zheng, Experimental studies on helical milling process to improve hole quality for the Superalloy (MSRR7197), Int. J. Adv. Manuf. Technol. 99 (2018) 1449–1458, https://doi.org/10.1007/s00170-018-2588-3.
[29] D. Sun, P. Lemoine, D. Keys, P. Doyle, S. Malinov, Q. Zhao, X. Qin, Y. Jin, Hole-making processes and their impacts on the microstructure and fatigue response of aircraft alloys, Int. J. Adv. Manuf. Technol. 94 (2018) 1719–1726, https://doi.org/10.1007/s00170-016-9850-3.
[30] S. Akula, S.N. Nayak, G. Bolar, V. Managuli, Comparison of conventional drilling and helical milling for hole making in Ti6Al4V titanium alloy under sustainable dry condition, Manuf. Rev. 8 (2021) 12, https://doi.org/10.1051/mfreview/2021010.

[31] A.J. Festas, R.B. Pereira, A. Ramos, J.P. Davim, A study of the effect of conventional drilling and helical milling in surface quality in titanium Ti-6Al-4V and Ti-6AL-7Nb alloys for medical applications, Arabian J. Sci. Eng. 46 (2021) 2361–2369, https://doi.org/10.1007/s13369-020-05047-8.
[32] A.C. Alvim, J.R. Ferreira, R.B.D. Pereira, The enhanced normalized normal constraint approach to multi-objective robust optimization in helical milling process of AISI H13 hardened with crossed array, Int. J. Adv. Manuf. Technol. 119 (2022) 2763–2784, https://doi.org/10.1007/s00170-021-08259-w.
[33] G. Bolar, R. Adhikari, S.N. Nayak, S.N. Joshi, Assessment of ignition risk in dry helical hole milling of AZ31 magnesium alloy considering the machining temperature and chip morphology, J. Manuf. Process. 77 (2022) 260–271, https://doi.org/10.1016/j.jmapro.2022.03.023.
[34] B. Denkena, D. Boehnke, J.H. Dege, Helical milling of CFRP–titanium layer compounds, CIRP J. Manuf. Sci. Technol. 1 (2008) 64–69, https://doi.org/10.1016/j.cirpj.2008.09.009.
[35] A. Abidi, S. Ben Salem, M.A. Yallese, Machining quality of high speed helical milling of carbon fiber reinforced plastics, Proc. Inst. Mech. Eng. C: J. Mech. Eng. Sci. 236 (2022) 1049–1066, https://doi.org/10.1177/0954406221996736.
[36] B. Wang, Y. Wang, H. Zhao, L. Sun, M. Wang, X. Kong, Effect of a Ti alloy layer on CFRP hole quality during helical milling of CFRP/Ti laminate, Compos. Struct. 252 (2020), 112670, https://doi.org/10.1016/j.compstruct.2020.112670.
[37] B. Wang, H. Zhao, F. Zhang, M. Wang, Y. Zheng, Comparison of the geometric accuracy of holes made in CFRP/Ti laminate by drilling and helical milling, Int. J. Adv. Manuf. Technol. 112 (2021) 3343–3350, https://doi.org/10.1007/s00170-021-06594-6.
[38] B. Wang, Y. Wang, H. Zhao, M. Wang, L. Sun, Mechanisms and evaluation of the influence of cutting temperature on the damage of CFRP by helical milling, Int. J. Adv. Manuf. Technol. 113 (2021) 1887–1897, https://doi.org/10.1007/s00170-021-06745-9.
[39] G. Bolar, A.K. Sridhar, A. Ranjan, Drilling and helical milling for hole making in multi-material carbon reinforced aluminum laminates, Int. J. Lightweight Mater. Manuf. 5 (2022) 113–125, https://doi.org/10.1016/j.ijlmm.2021.11.004.
[40] R.B.D. Pereira, R.R. Leite, A.C. Alvim, A.P. de Paiva, J.R. Ferreira, J.P. Davim, Multi-objective robust optimization of the sustainable helical milling process of the aluminum alloy Al 7075 using the augmented-enhanced normalized normal constraint method, J. Clean Prod. 152 (2017) 474–496, https://doi.org/10.1016/j.jclepro.2017.03.121.
[41] R.B.D. Pereira, R.R. Leite, A.C. Alvim, A.P. de Paiva, P.P. Balestrassi, J.R. Ferreira, J.P. Davim, J. Multivariate robust modeling and optimization of cutting forces of the helical milling process of the aluminum alloy Al 7075, Int. J. Adv. Manuf. Technol. 95 (2018) 2691–2715, https://doi.org/10.1007/s00170-017-1398-3.
[42] J.A. Gonsalves, R. Adhikari, G. Bolar, Comparative evaluation of hole making processes in magnesium alloy AZ31 under dry machining condition, Mater. Today Proc. 46 (2021) 4356–4361, https://doi.org/10.1016/j.matpr.2020.09.662.
[43] C. Ji, Y. Li, X. Qin, Q. Zhao, D. Sun, Y. Jin, 3D FEM simulation of helical milling hole process for titanium alloy Ti-6Al-4V, Int. J. Adv. Manuf. Technol. 81 (2015) 1733–1742, https://doi.org/10.1007/s00170-015-7323-8.
[44] A.K. Parida, Simulation and experimental investigation of drilling of Ti-6Al-4V alloy, Int. J. Lightweight. Mater. Manuf. 1 (2018) 197–205, https://doi.org/10.1016/j.ijlmm.2018.07.001.
[45] M. Kuntoğlu, H. Sağlam, ANOVA and fuzzy rule-based evaluation and estimation of flank wear, temperature and acoustic emission in turning, CIRP J. Manuf. Sci. Technol. 35 (2021) 589–603, https://doi.org/10.1016/j.cirpj.2021.07.011.
[46] A. Rasti, M.H. Sadeghi, S.S. Farshi, An investigation into the effect of surface integrity on the fatigue failure of AISI 4340 steel in different drilling strategies, Eng. Fail. Anal. 95 (2019) 66–81, https://doi.org/10.1016/j.engfailanal.2018.08.022.
[47] M.A. Yallese, K. Chaoui, N. Zeghib, L. Boulanouar, J.F. Rigal, Hard machining of hardened bearing steel using cubic boron nitride tool, J. Mater. Process. Technol. 209 (2009) 1092–1104, https://doi.org/10.1016/j.jmatprotec.2008.03.014.
[48] S. Bi, J. Liang, Experimental studies and optimization of process parameters for burrs in dry drilling of stacked metal materials, Int. J. Adv. Manuf. Technol. 53 (2011) 867–876, https://doi.org/10.1007/s00170-010-2877-y.
[49] H. Wang, X. Qin, C. Ren, Q. Wang, Prediction of cutting forces in helical milling process, Int. J. Adv. Manuf. Technol. 58 (2012) 849–859, https://doi.org/10.1007/s00170-011-3435-y.
[50] Z. Li, Q. Liu, X. Ming, X. Wang, Y. Dong, Cutting force prediction and analytical solution of regenerative chatter stability for helical milling operation, Int. J. Adv. Manuf. Technol. 73 (2014) 433–442, https://doi.org/10.1007/s00170-014-5793-8.
[51] V. Marakini, S.P. Pai, U.K. Bhat, D.S. Thakur, B.P. Achar, High-speed face milling of AZ91 Mg alloy: surface integrity investigations. Int. J. Lightweight Mater. Manuf. 5 (2022), 528-542. https://doi.org/10.1016/j.ijlmm.2022.06.006.
[52] H.A. Al-Tameemi, T. Al-Dulaimi, M.O. Awe, S. Sharma, D.Y. Pimenov, U. Koklu, K. Giasin, Evaluation of cutting-tool coating on the surface roughness and hole dimensional tolerances during drilling of Al6061-T651 alloy, Materials 14 (2021) 1783, https://doi.org/10.3390/ma14071783.
[53] G. Bolar, A. Das, S.N. Joshi, Measurement and analysis of cutting force and product surface quality during end-milling of thin-wall components, Measurement 121 (2018) 190–204, https://doi.org/10.1016/j.measurement.2018.02.015.
[54] M.H. Saadatbakhsh, H. Imani, M.H. Sadeghi, S.S. Farshi, Experimental study of surface roughness and geometrical and dimensional tolerances in helical milling of AISI 4340 alloy steel, Int. J. Adv. Manuf. Technol. 93 (2017) 4063–4074, https://doi.org/10.1007/s00170-017-0782-3.
[55] Ü.A. Usca, M. Uzun, S. Şap, M. Kuntoğlu, K. Giasin, D.Y. Pimenov, S. Wojciechowski, Tool wear, surface roughness, cutting temperature and chips morphology evaluation of Al/TiN coated carbide cutting tools in milling of Cu–B–CrC based ceramic matrix composites, J. Mater. Res. Technol. 16 (2022) 1243–1259, https://doi.org/10.1016/j.jmrt.2021.12.063.
[56] D. Carou, E.M. Rubio, C.H. Lauro, J.P. Davim, Experimental investigation on finish intermittent turning of UNS M11917 magnesium alloy under dry machining, Int. J. Adv. Manuf. Technol. 75 (2014) 1417–1429, https://doi.org/10.1007/s00170-014-6215-7.
[57] S. Amini, M. Baraheni, E. Hakimi, Enhancing dimensional accuracy and surface integrity by helical milling of carbon fiber reinforced polymers, Int. J. Lightweight Mater. Manuf. 2 (2019) 362–372, https://doi.org/10.1016/j.ijlmm.2019.03.001.
[58] X. Cui, J. Zhao, C. Jia, Y. Zhou, Surface roughness and chip formation in high-speed face milling AISI H13 steel, Int. J. Adv. Manuf. Technol. 61 (2012) 1–13, https://doi.org/10.1007/s00170-011-3684-9.
[59] K. Shi, D. Zhang, J. Ren, Optimization of process parameters for surface roughness and microhardness in dry milling of magnesium alloy using Taguchi with grey relational analysis, Int. J. Adv. Manuf. Technol. 81 (2015) 645–651, https://doi.org/10.1007/s00170-015-7218-8.